Steady Characteristics of High-Speed Micro-Gas Journal Bearings With Different Gaseous Lubricants and Extreme Temperature Difference

Xueqing Zhang
Key Laboratory of Low-Grade Energy Utilization Technologists and Systems of Ministry of Education, College of Power Engineering, Chongqing University, Chongqing 40030, China
e-mail: xueqingzhang@cqu.edu.cn

Qinghua Chen
Mem. ASME
Key Laboratory of Low-Grade Energy Utilization Technologists and Systems of Ministry of Education, College of Power Engineering, Chongqing University, Chongqing 40030, China
e-mail: qhchen@cqu.edu.cn

Juanfang Liu[1]
Key Laboratory of Low-Grade Energy Utilization Technologists and Systems of Ministry of Education, College of Power Engineering, Chongqing University, Chongqing 40030, China
e-mail: juanfang@cqu.edu.cn

High-speed micro-gas journal bearing is one of the essential components of micro-gas turbines. As for the operating conditions of bearings, the high-speed, high-temperature, ultra-high temperature difference along the axial direction and the species of gaseous lubricants are extremely essential to be taken into account, and the effects of these factors are examined in this paper. The first-order modified Reynolds equation including the thermal creep, which results from the extremely large temperature gradient along the axial direction, is first derived and coupled with the simplified energy equation to investigate the steady hydrodynamic characteristics of the micro-gas bearings. Under the isothermal condition, it is found that CO_2 can not only improve the stability of bearings but also generate a relatively higher load capacity by some comparisons. Thus, CO_2 is chosen as the lubricant to further explore the influence of thermal creep. As the rotation speed and eccentricity ratio change, the thermal creep hardly has any effect on the gas film pressure. However, the shorter bearing length can augment the thermal creep. Compared with the cases without the thermal creep, the thermal creep could remarkably destroy the stability of gas bearing, but it might slightly enhance the load capacity.
[DOI: 10.1115/1.4033565]

Keywords: hydrodynamic characteristics, species of gaseous lubricants, extreme temperature difference, thermal creep

Introduction

After an original concept on microelectromechanical systems (MEMS), power systems were proposed by Epstein et al. [1], and the systems have been studied at MIT since 1994. The micro-gas turbine is a typical MEMS power system and designed to produce an electric power of about 10–20 W or the thrust of about 0.05–0.1 N. Such high power density requires combustor exit temperatures of 1300–1700 K, rotor peripheral speeds of 300–600 m/s, tight clearances between rotating and static parts ($<5\,\mu$m), and thermal isolation of the hot and cold sections. A 100 W class microscale gas turbine has been designed and verified by Isomura et al. [2] in Japan. In this device, the combustor exit temperature reaches up to 1050 °C and the rotor is required to rotate at 870,000 rpm. Although the bearing gas comes from the compressor side, heat transfer from the combustor to the turbine makes the gas film temperature reach up to 200–300 °C. In Belgium, Peirs et al. [3] designed a portable gas turbine generator, which can generate electrical power of 16 W and the turbine has been tested at temperature up to 360 °C and speed up to 160,000 rpm.

For the micro-gas turbines, the high-speed micro-gas journal bearing is one of the necessary components, which connects the turbine expander with the compressor in a tight space. Hence, the gas-lubricated film has an extremely high-temperature gradient along the axial direction owing to the large temperature difference between the turbine expander exit and the compressor inlet. Generally, the gaseous lubricant comes from the exhaust gas of the combustor, so the temperature can reach up to several hundred degree Celsius [1]. Moreover, the gaseous lubricant is a multicomponent mixture and the components are dependent on the combustion products. Therefore, it is extremely essential to take into account the effects of the high temperature, the multicomponent gas lubrication, and the larger temperature difference along the axial direction on the hydrodynamic properties. However, these factors are generally ignored in the existing researches.

Piekos [4] argued that the higher gas pressure in the microturbine makes the mean free path (MFP) of gas molecules to reduce and the Knudsen number to less than 0.01, and thus, the velocity slip can be ignored. But the gas bearing is assumed to operate at the room temperature. Lee et al. [5] compared the static and dynamic characteristics for slip flow at room temperature with those at high temperature in a range of bearing numbers. The results demonstrated that the effect of slip flow became significant at the higher temperature as well as at the lower bearing numbers. Zhang et al. [6] proposed a modified Reynolds equation based on Burgdorfer's first-order slip boundary condition at the different temperatures. Their numerical analysis showed that the gas film pressure and nondimensional load capacities markedly decreased as the gas rarefaction effect increased. Zhang et al. [7] analyzed the static performance of microbearings by using the spectral collocation method. The results showed that the load capacity increased with the increase in the lower operating temperature and the temperature dependence of the load capacity became weaker at the higher temperature. Zhang et al. [8] coupled the molecular gas-film lubrication equation with the kinetic equations to study the characteristics of bearing–rotor systems and found that the temperature range could be divided into two regions: the viscosity effect dominant region and the rarefaction effect dominant region.

In this study, we first compare the viscosity and reference Knudsen number of the different gaseous lubricants. Furthermore, the first-order modified Reynolds equation with the thermal creep is derived and coupled with the simplified energy equation.

[1]Corresponding author.

Contributed by the Tribology Division of ASME for publication in the JOURNAL OF TRIBOLOGY. Manuscript received November 21, 2015; final manuscript received April 19, 2016; published online August 11, 2016. Assoc. Editor: Bugra Ertas.

By using the previous controlling equations, the load capacity and attitude angle for the different gaseous lubricants are computed under the isothermal condition. Finally, CO_2 is chosen as the lubricant to compare the hydrodynamic characteristics of the gas bearings between the models with and without the thermal creep.

Viscosity and Reference Knudsen Number of the Different Gaseous Lubricants

According to the lubrication theory on the gas film, the reference Knudsen number of micro-gas journal bearings can be defined as $\mathrm{Kn}_0 = \lambda_a / h_{\min}$. In which, $h_{\min}$ is the minimum gas film thickness and λ_a is the MFP of gas molecules at the ambient pressure and can be calculated as

$$\lambda_a = \mu\sqrt{\pi RT}/\sqrt{2M}p_a \tag{1}$$

where μ is the dynamic viscosity, R is the gas constant and equal to 8.31441 $\mathrm{J/(mol\,K)}$, T is the gas film temperature, M is the molar mass, and p_a is the ambient pressure and set to 1.01×10^5 $\mathrm{N/m^2}$. The gas viscosity is calculated by the following Sutherland-law formulation:

$$\mu(T) = \mu_0 \left(\frac{T}{T_0}\right)^{1.5} \left(\frac{T_0 + T_s}{T + T_s}\right) \tag{2}$$

where μ_0 is the dynamic viscosity at 0 °C, T_0 is equal to 273.16 K, and T_s is the Sutherland constant and related to the gas species (see Table 1) [9–12].

Figure 1 displays the change of μ as a function of the temperature. It can be observed that the viscosity of each gas presents an increasing trend with the gas temperature. In which, the viscosity is obtained by Eq. (2). In fact, according to the knowledge of gas dynamics, the gas viscosity is proportional to the gas molar mass and temperature and inversely proportional to the gas effective molecular diameter. For a given lubricant, the gas viscosity is only dependent on the temperature. Therefore, the increase in the gas temperature leads to a larger gas viscosity. Among the listed gases, the change in the viscosity of H_2O is most acute with the temperature and hydrogen is weakest. At a given temperature, the oxygen viscosity is largest and the hydrogen viscosity is smallest. It is attributed to the competition between the contribution of the molar mass and the gas molecular effective diameter to the gas viscosity (see Table 1).

Table 1 Dynamic viscosity at 0 °C μ_0, the Sutherland-law constant T_s, and the effective molecular diameter d for the different gases

Gas	μ_0(N s/m^2)	T_s (K)	d (m)
H_2	0.84×10^{-5}	71	2.7×10^{-10}
CH_4	1.0198×10^{-5}	164	3.8×10^{-10}
O_2	1.92×10^{-5}	125	3.6×10^{-10}
H_2O	0.893×10^{-5}	961	3.0×10^{-10}
CO_2	1.38×10^{-5}	254	4.6×10^{-10}

If the minimum gas film thickness $h_{\min}$ is set to 1 μm, the reference Knudsen numbers, denoted by Kn_0, for the different gases are plotted in Fig. 2. It can be observed that the reference Knudsen number increases as the gas film temperature is elevated, since the MFP of gas molecules increases. It implies that the higher temperature can result in the more remarkable rarefaction effect. The MFP of the gas molecules is proportional to the gas viscosity and inversely proportion to the molar mass of the different gaseous lubricants at a specific temperature. Therefore, the change in the viscosity of H_2O leads to a significant change in the reference Knudsen number of H_2O with the gas temperature. Also, Kn_0 of H_2 is largest and the one of CO_2 is smallest.

Methodology. According to the calculation, Kn_0 is far larger than 0.01 in the operating temperature range, so that the slip must be considered in the high-speed micro-gas bearings. When the rarefaction effect cannot be neglected, the temperature gradient along the surfaces of rotor and stator can make the gas inside the bearings flow from the low-temperature end to the high-temperature end, the thermal creep occurs. To derive the first-order modified Reynolds equation including the thermal creep in the axial direction (y-coordinate), the model of gas journal bearings and a three-dimensional gas film lubrication is schematically shown in Fig. 3. In the model, the outer ring is the stator and the inner is the rotor with a radius of r, which rotates at a speed of ω. The low-temperature end (the compressor side) is located at $y = -L/2$, and the high-temperature end (the turbine expander side) is at $y = L/2$.

The following assumptions are made: (i) the gas pressure is constant across the film and (ii) the pressure and the viscous force balance in the circumferential and axial directions. Hence, the momentum equation describing the gas lubrication can be simplified as

$$\frac{\partial p}{\partial \theta} = r\frac{\partial}{\partial z}\left(\mu\frac{\partial u}{\partial z}\right) \tag{3}$$

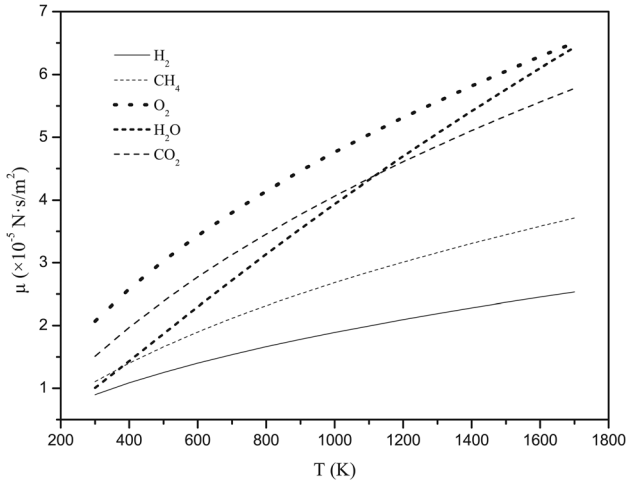

Fig. 1 Variation in the dynamic viscosity with the gas film temperature for the different gaseous lubricants

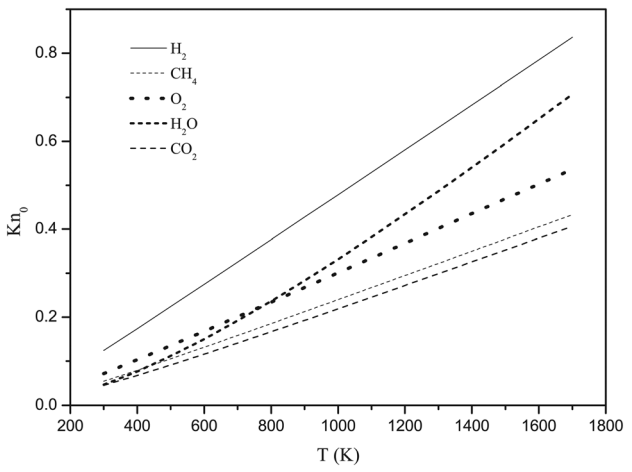

Fig. 2 Variation in the reference Knudsen number with the gas film temperature for the different gaseous lubricants

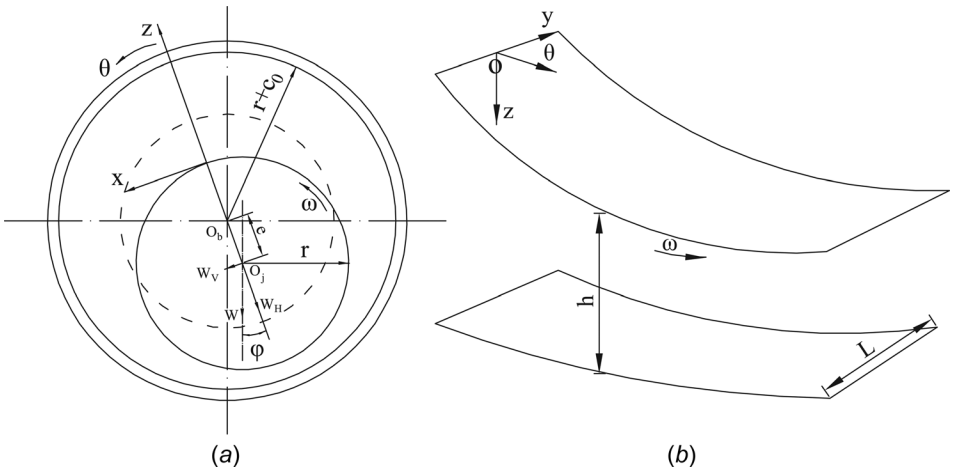

Fig. 3 Schematic of the gas journal bearings (*a*) and three-dimensional coordinates of the gas film (*b*)

$$\frac{\partial p}{\partial z} = 0 \tag{4}$$

$$\frac{\partial p}{\partial y} = \frac{\partial}{\partial z}\left(\mu \frac{\partial v}{\partial z}\right) \tag{5}$$

where θ, y, and z are the circumferential, axial, and radial coordinates, respectively.

Based on Maxwell's first-order slip model [13], the velocities on the boundary in the circumferential (θ coordinate) and axial directions (y-coordinate) are given by

$$\begin{aligned} u_{z=0} &= \omega r + \lambda \left.\frac{du}{dz}\right|_{z=0} \\ u_{z=h} &= -\lambda \left.\frac{du}{dz}\right|_{z=h} \end{aligned} \tag{6}$$

$$\begin{aligned} v_{z=0} &= \lambda \left.\frac{dv}{dz}\right|_{z=0} + \frac{3}{4}\left(\frac{\mu}{\rho T}\right)_{z=0}\left(\frac{\partial T}{\partial y}\right)_{z=0} \\ v_{z=h} &= -\lambda \left.\frac{dv}{dz}\right|_{z=h} + \frac{3}{4}\left(\frac{\mu}{\rho T}\right)_{z=h}\left(\frac{\partial T}{\partial y}\right)_{z=h} \end{aligned} \tag{7}$$

where u and v are the velocities in the circumferential and axial directions, respectively. λ is the MFP of gas molecules that is calculated using $\lambda = \mu\sqrt{\pi RT}/\sqrt{2M}p$, where p is the gas film pressure, and ρ is the gas density.

Combining the boundary conditions, Eqs. (3) and (5) are integrated, and the following velocity equations in the circumferential and axial directions, respectively, are yielded:

$$u = -\frac{1}{2\mu r}\frac{\partial p}{\partial \theta}\quad (h\lambda + hz - z^2) + \omega r\left(1 - \frac{z+\lambda}{h+2\lambda}\right) \tag{8}$$

$$\begin{aligned} v = &-\frac{1}{2\mu}\frac{\partial p}{\partial y}\quad (h\lambda + hz - z^2) \\ &+ \left(1 - \frac{\lambda + z}{h+2\lambda}\right)\frac{3}{4}\left(\frac{\mu}{\rho T}\right)_{z=0}\left(\frac{\partial T}{\partial y}\right)_{z=0} \\ &+ \frac{\lambda + z}{h+2\lambda}\frac{3}{4}\left(\frac{\mu}{\rho T}\right)_{z=h}\left(\frac{\partial T}{\partial y}\right)_{z=h} \end{aligned} \tag{9}$$

$$h = c_0(1 + \varepsilon\cos\theta) \tag{10}$$

$$\varepsilon = e/c_0 \tag{11}$$

where h is the gas film thickness, c_0 is the radius clearance, ε is the eccentricity ratio, and e is the eccentric distance.

The gas film temperature gradient on the rotor surface is assumed to be equal to that on the stator surface, $(3/4)(\mu/\rho T)_{z=0}(\partial T/\partial y)_{z=0} = (3/4)(\mu/\rho T)_{z=h}(\partial T/\partial y)_{z=h}$. Hence, the velocity equation in the axial direction can be further simplified as

$$v = -\frac{1}{2\mu}\frac{\partial p}{\partial y}\quad (h\lambda + hz - z^2) + \frac{3}{4}\left(\frac{\mu}{\rho T}\right)_{z=0}\left(\frac{\partial T}{\partial y}\right)_{z=0} \tag{12}$$

Substituting Eqs. (8)–(12) into the continuity equation and integrating across the gas film, the following first-order modified Reynolds equation with the thermal creep are obtained:

$$\begin{aligned} &\frac{\partial}{\partial \theta}\left[\frac{p}{\mu T_m}(h^3 + 6\lambda h^2)\frac{\partial p}{\partial \theta}\right] + r^2\frac{\partial}{\partial y}\left[\frac{p}{\mu T_m}(h^3 + 6\lambda h^2)\frac{\partial p}{\partial y}\right] \\ &\quad = 6\omega r^2\frac{\partial}{\partial \theta}\left(\frac{ph}{T_m}\right) + 9r^2\left(\frac{\mu}{\rho T}\right)_{z=0}\left(\frac{\partial T}{\partial y}\right)_{z=0}\frac{\partial}{\partial y}\left(\frac{ph}{T_m}\right) \end{aligned} \tag{13}$$

where T_m is the averaged cross-film gas temperature.

If the temperature change in the gas film is considered, in order to attain the gas film temperature profiles, Eq. (13) is needed to be coupled with the energy equation. The following simplified energy equation is adopted [14]:

$$\begin{aligned} \rho c_p\left(u\frac{\partial T}{r\partial \theta} + v\frac{\partial T}{\partial y}\right) = &\, k\left(\frac{1}{r^2}\frac{\partial^2 T}{\partial \theta^2} + \frac{\partial^2 T}{\partial y^2} + \frac{\partial^2 T}{\partial z^2}\right) \\ &+ \left(\frac{u}{r}\frac{\partial p}{\partial \theta} + v\frac{\partial p}{\partial y}\right) + \mu\left[\left(\frac{\partial u}{\partial z}\right)^2 + \left(\frac{\partial v}{\partial z}\right)^2\right] \end{aligned} \tag{14}$$

where c_p is the constant pressure specific heat, and k is the thermal conductivity.

The load capacity of the hydrodynamic gas journal bearings consists of two parts. One is along the line of centers (W_H) and the other is perpendicular to the line of centers (W_V), as shown in Fig. 3(*a*). The attitude angle (φ) and the dimensionless load capacity (W) are calculated by the following formulations:

$$W_H = 2\int_0^{L/2}\int_0^{2\pi} p\cos\theta r d\theta dy \tag{15}$$

$$W_V = 2\int_0^{L/2}\int_0^{2\pi} p\sin\theta r d\theta dy \tag{16}$$

$$W = \sqrt{W_H^2 + W_V^2}/(p_a 2\pi r L) \tag{17}$$

$$\varphi = \arctan(-W_V/W_H) \quad (\text{deg}) \tag{18}$$

The central difference scheme is used to discretize the above controlling equations. And the uniform grids are meshed in the computational domain. The convergence criteria of the results are measured by

$$\text{Error} = \left| \frac{\sum(\varphi_{\text{new}} - \varphi)}{\sum \varphi_{\text{new}}} \right| < 10^{-10} \tag{19}$$

where $\varphi \in \{p, T\}$ and φ_{new} are the corresponding updated values at each interactions.

Results and Discussion

Effect of the Different Gaseous Lubricants. In order to perform a straight comparison of the steady characteristics for the different gaseous lubricants, the gas film is assumed to be isothermal and the thermal creep is not considered. The main geometrical parameters of the gas bearing are given as $r = 2.0 \times 10^3$ μm, $c_0 = 10$ μm, and $L = 300$ μm, and the gas film temperature is set to 1100 K. The corresponding pressure boundary conditions are given as follows:

$$p(\theta, \pm L/2) = p_a, \quad p(\theta, y) = p(\theta, -y) \tag{20}$$

In Fig. 4, raising the rotation speed brings about a sharp enhancement of the load capacity for each gaseous lubricant. The load capacity of O_2 is highest, and that of H_2 is lowest. In addition, the load capacity of H_2O is higher than that of CH_4 and lower than that of CO_2. This order is consistent with that of the corresponding gas viscosity at $T = 1100K$, namely, the gaseous lubricant with the larger viscosity can obtain a higher load capacity. However, the larger the Knudsen number of gaseous lubricant is, the greater the weakening effect of rarefaction on the load capacity. Although the viscosity of CO_2 is far smaller than that of O_2, the load capacity of CO_2 is just a little lower than that of O_2. It is attributed to the fact that the rarefaction effect of O_2 is higher than that of CO_2. Additionally, CO_2 just has a little higher viscosity than H_2O at $T = 1100$ K, but it has a far higher load capacity than H_2O. This is because the rarefaction effect of H_2O is much higher than that of CO_2 at $T = 1100$ K. Therefore, for the different gaseous lubricants, the magnitude of load capacity is dependent on the combined impact of the gas viscosity and the rarefaction effect.

In Fig. 5, the attitude angle decreases as the rotation speed is elevated. When the speed is relatively lower, the decrease in the attitude angle presents a sharp trend. Upon increasing the speed,

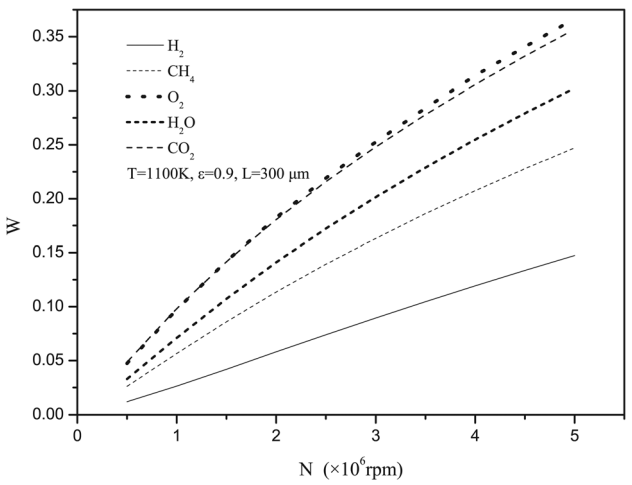

Fig. 4 Variation of the load capacity with the rotation speed for the different gaseous lubricants

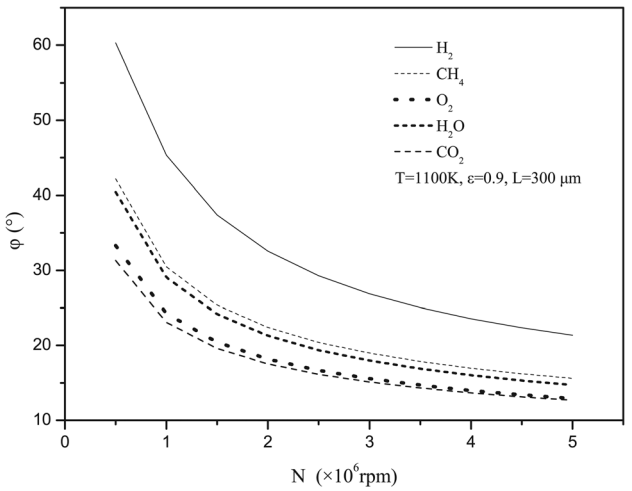

Fig. 5 Variation of the attitude angle with the rotation speed for the different gaseous lubricants

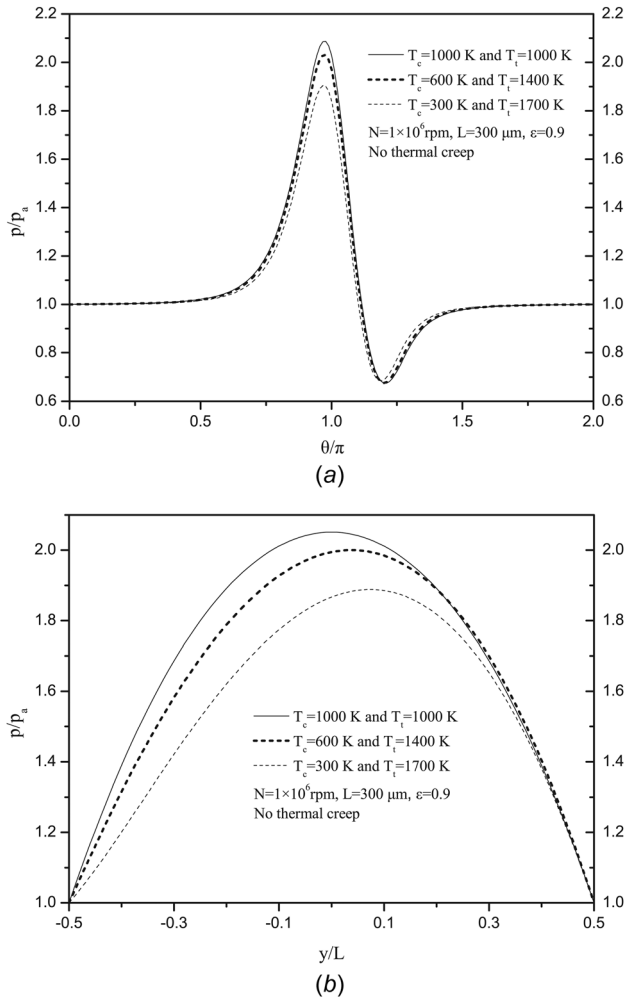

Fig. 6 Profiles of the gas film pressure at the different temperatures: (*a*) $y = 0$ and (*b*) $\theta = \pi$

Table 2 *W* and φ at the different temperature differences

Temperature difference	W	φ (deg)
$T_c = 1000\,\mathrm{K}$ and $T_t = 1000\,\mathrm{K}$	0.02714	28.71547
$T_c = 600\,\mathrm{K}$ and $T_t = 1400\,\mathrm{K}$	0.02516	29.46237
$T_c = 300\,\mathrm{K}$ and $T_t = 1700\,\mathrm{K}$	0.02085	31.45887

the decrease becomes slower. According to the knowledge of hydrodynamics, the smaller attitude angle can improve the stability of gas bearings due to the smaller counterforce perpendicular to the line of centers [15]. Hence, the higher rotation speed is beneficial to the stable operation of the bearings. At the same speed, the attitude angle reduces with the increase in the gas molar mass, since the larger molecular mass can make the gas film possess a larger inertia. And thus, the counterforce of the gas film is not easy to form the normal component and the stability of bearings is more excellent. Among the considered gases, the molar mass of CO_2 is largest, so its attitude angle is smallest.

Effect of the Temperature Gradient Along the Axial Direction. In this section, the first-order modified Reynolds equation coupled with the simplified energy equation is adopted to analyze the hydrodynamic characteristics of gas journal bearings. Based on the above results, CO_2 is selected as the lubricant, because it can result in a relatively higher load capacity and a smaller attitude angle compared with the other gases. In addition, it is also a kind of combustion product. c_p and k are the functions of temperature and they are obtained using the following equations [9–12]:

$$k(T) = 0.01456\left(\frac{T}{T_0}\right)^{1.5}\left(\frac{T_0 + 2222}{T + 2222}\right) \quad (\mathrm{W/(m\,K)}) \tag{21}$$

$$c_p(T) = 872.5 + 0.2406(T - T_0) \quad (\mathrm{J/(kg\,K)}) \tag{22}$$

The corresponding pressure and temperature boundary conditions are given as

$$\begin{aligned} p(\theta, \pm L/2) &= p_a, \quad p(\theta, y) = p(\theta, -y) \\ T(\theta, -L/2) &= T_c, \quad T(\theta, L/2) = T_t \end{aligned} \tag{23}$$

To analyze the effects of the ultra-large temperature gradient along the axial direction on the hydrodynamic properties of gas bearings, the thermal creep is not considered first. Figure 6 presents the pressure profiles of gas film in the circumferential and axial directions. It can be seen that the larger the temperature difference is, the lower the gas film pressure is. So, the load capacity is also reduced (see Table 2). This is because of the fact that the larger temperature difference between the compressor and the turbine expander enhances the heat transfer between them. Therefore, the heat generated by the viscous dissipation is more easily taken away. However, the heat absorbed from the higher temperature end cannot be transformed into the kinetic energy of gas film. So, the viscous dissipation would more significantly reduce the gas film pressure at the larger temperature difference. In addition, based on the thermodynamics, the increase in the temperature difference between the compressor side and the turbine expander side leads to a larger irreversible loss, and thus, the

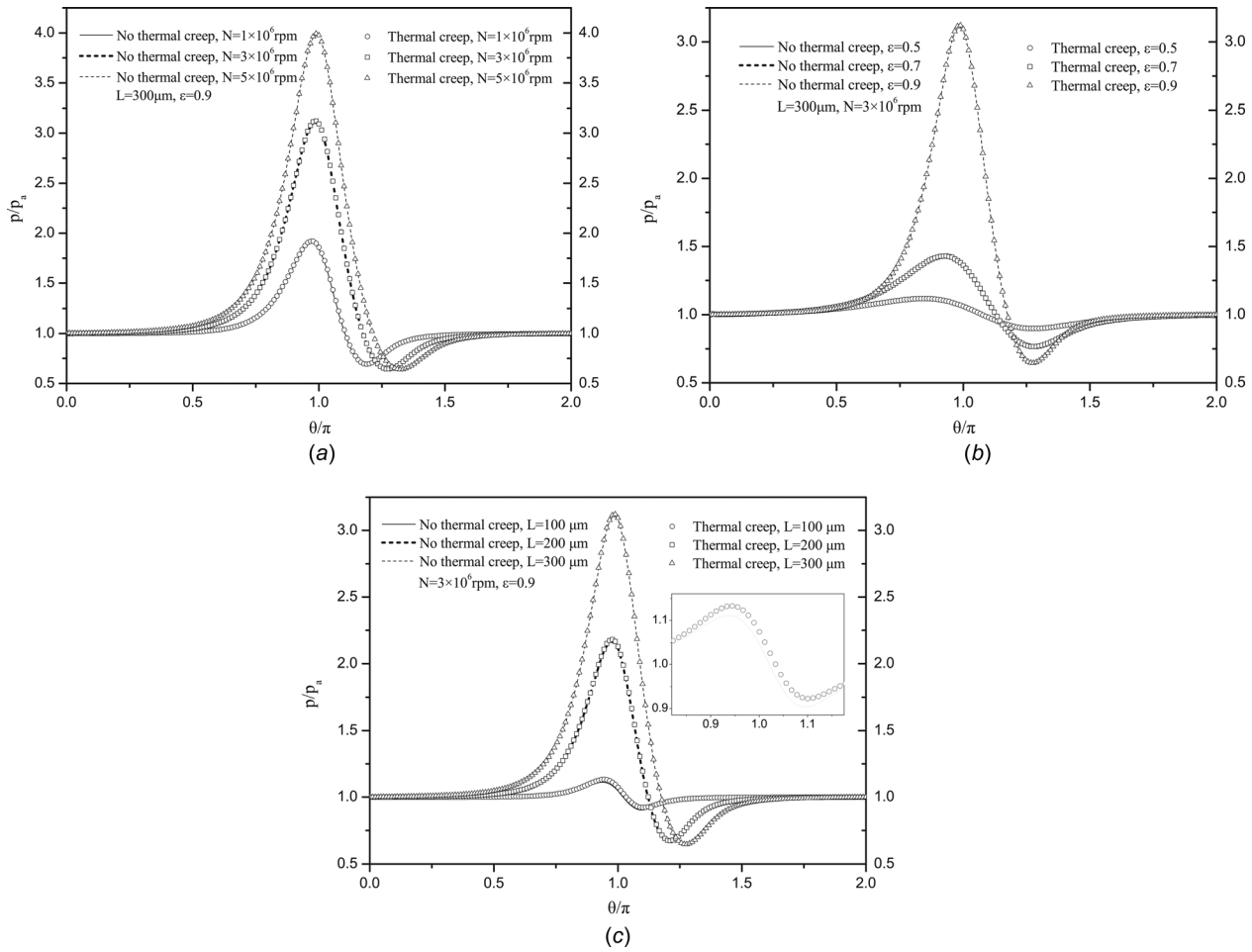

Fig. 7 Comparison of the film pressure profiles at the different rotation speeds (*a*), eccentricity ratios (*b*), and bearing lengths (*c*)

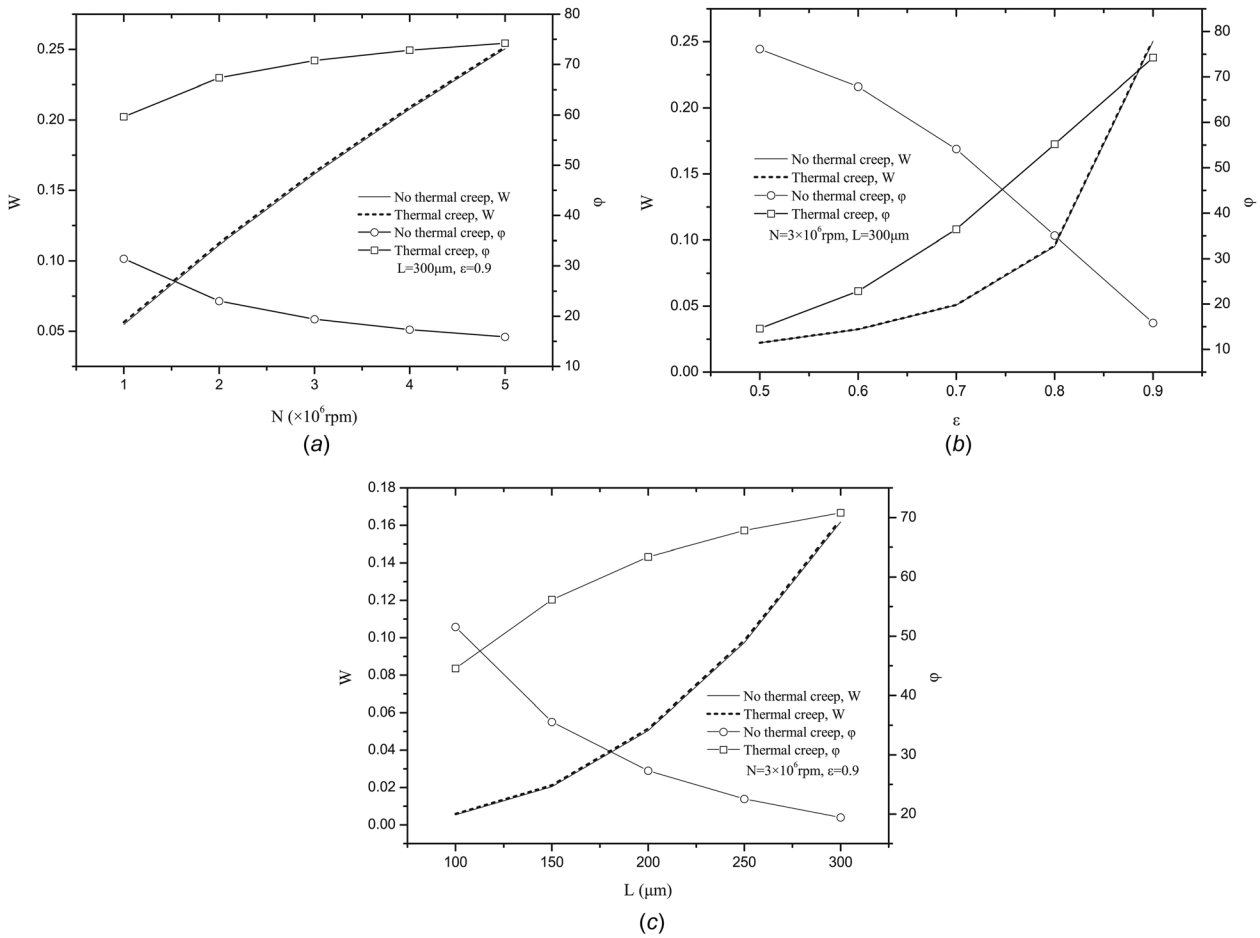

Fig. 8 Variations in the load capacity and the attitude angle with (*a*) the rotation speed, (*b*) the eccentricity ratio, and (*c*) the bearing length

useful work output declines. As the temperature difference increases, the pressure profile peak is more severely skewed toward the high-temperature end (see Fig. 6(*b*)) and the attitude angle increases (see Table 2), which might damage the stability of the gas bearings.

Under the condition of $T_c = 300\,\mathrm{K}$ and $T_t = 1700\,\mathrm{K}$, the comparison of the pressure profiles of gas film between with and without the thermal creep is shown in Fig. 7 at the different rotation speeds, eccentricity ratios, and bearing lengths. The changes in the eccentricity ratio and rotation speed lead to almost no difference in the pressure profiles between the two cases in which the thermal creep is considered and ignored. However, if the bearing length becomes shorter, the thermal creep causes the gas film pressure to be slightly enhanced due to the larger temperature gradient along the axial direction. From the enlarged portion in Fig. 7(*c*), it can be seen that the thermal creep can relatively improve the gas film pressure in the region from the gas film squeezed into the film expanded. In addition, utilizing the longer bearing generates the higher pressure. Therefore, the shorter bearing can sharply degrade the load capacity and further impact the operating performance of the bearing.

In Fig. 8, the load capacity can be significantly improved by the rotation speed, eccentricity ratio, and bearing length. From the figures, it can be seen that the load capacity with the thermal creep is slightly higher than one in the cases in which the thermal creep is not considered. However, the attitude angle is greatly distinct in the two cases with and without the thermal creep. The attitude angle remarkably declines with increasing the rotation speed, eccentricity ratio, and bearing length in the case of not considering the thermal creep, but the attitude angle presents a rising trend with the increase in the previous factors as the thermal creep is taken into account. It is note worthy that the attitude angles with the thermal creep are far higher than those without the thermal creep under the conditions of the higher rotation speed ($N > 10^6$ rpm), the larger eccentricity ratio ($\varepsilon > 0.75$), and the longer bearing length ($L > 110$ μm). Namely, the differences of the attitude angles between the two cases are much greater at the higher parameters. The effects of thermal creep on the load capacity and the attitude angle are mainly caused by the counterforce of thermal creep along the axial direction, which can increase the gas pressure. Additionally, as the gas pressure rises by the same amount, the integral value of Eq. (16) increases more than that of Eq. (15). Thus, both of the load capacity and the attitude angle with the thermal creep are larger than those without the thermal creep. Meantime, the increase in the rotation speed and eccentricity rate not only enhances the gas film pressure but also strengthens the counterforce of the thermal creep, while the increase in the bearing length enhances the former and decreases the latter. Hence, the effects of the thermal creep are more notable at the higher rotation speed and eccentricity rate, but they are weaker at the longer bearing length. The existence of the thermal creep extremely damages the stability of gas bearings and is destructive to the operation of gas bearings.

Conclusions

Based on the first-order modified Reynolds equation, the effects of the different gaseous lubricant species and the extreme temperature difference between the compressor side and the turbine

expander side on the steady characteristics of the micro-gas bearings are mainly investigated. For a given lubricant, the gas viscosity and rarefaction effect dominate the magnitude of load capacity. Among the considered gaseous lubricants, CO_2 gas can significantly improve the stability of gas bearings due to its larger molar mass. The larger temperature difference between the compressor side and the turbine expander side gives rise to the lower pressure of gas film. Moreover, the larger temperature difference can make the peak of the pressure profiles along the axial direction severely skewed toward the higher temperature end and it is unfavorable for the stability of gas bearings. By comparing the film pressures, it is found that the changes of eccentricity ratio and rotation speed hardly have any influence on the thermal creep, while the shorter bearing can enhance the thermal creep. The thermal creep slightly elevates the load capacity, compared with the case without the thermal creep. Additionally, the thermal creep extremely degrades the stability of gas bearings in the case that the rotation speed is more than 10^6 rpm, the eccentricity ratio is more than 0.75, and the bearing length is more than 110 μm.

Acknowledgment

This work was supported by the National Science Foundation of China (Grant No. NSFC51206196) and the Fundamental Research Funds for the Central Universities (Grant No. CDJZR14140001).

Nomenclature

c_p = lubricated gas-specific heat at constant pressure ($\mathrm{J/(kg\,K)}$)
c_0 = radius clearance (μm)
e = eccentric distance (μm)
h = gas film thickness (μm)
$h_{\min}$ = minimum gas film thickness (μm)
k = gas film thermal conductivity (W/m K)
Kn_o = reference Knudsen number
L = bearing length (μm)
M = gas molar mass (kg/mol)
p = gas film pressure (Pa)
p_a = ambient pressure (Pa)
r = radius of the rotor (μm)
R = gas constant, $R = 8.31441\ \mathrm{J/(mol\,K)}$
T = gas film temperature (K)
T_c = compressor inlet temperature (K)
T_m = averaged cross-film temperature (K)
T_s = Sutherland constant (K)
T_t = turbine expander outlet temperature (K)
T_0 = Kelvin temperature at 0 °C (K)
u = gas film velocity in the circumferential direction (m/s)
v = gas film velocity in the axial direction (m/s)
W = dimensionless load capacity
W_H = load capacity along the line of centers (N)
W_V = load capacity perpendicular to the line of centers (N)
y, z = coordinates in the axial and film thickness direction

Greek Symbols

ε = eccentricity ratio
θ = coordinate in the circumferential direction
λ = mean free path of gas molecules (m)
λ_a = mean free path of gas molecules at the ambient pressure (m)
μ = lubricated gas dynamic viscosity (Pa·s)
μ_0 = lubricated gas dynamic viscosity as temperature is 0 °C (Pa·s)
ρ = lubricated gas density ($\mathrm{kg/m^3}$)
φ = attitude ratio (rad)
ω = angular velocity of the rotor (rad/s)

Subscripts

a = ambient
c = compressor
m = mean
min = minimum
t = turbine expander

References

[1] Epstein, A. H., Senturia, S. D., Al-Midani, O., Anathasuresh, G., Ayon, A., Breuer, K., Chen, K.-S., Ehrich, F. E., Esteve, E., Frechette, L., Gauba, G., Ghodssi, R., Groshenry, C., Jacobson, S., Kerrebrock, J. L., Lang, J. H., Lin, C.-C., London, A., Lopata, J., Mehra, A., Mur Miranda, J. O., Nagle, S., Orr, D. J., Piekos, E., Schmidt, M. A., Shirley, G., Spearing, S. M., Tan, C. S., Tzeng, Y.-S., and Waitz, I. A., 1997, "Micro-Heat Engines, Gas Turbines, and Rocket Engines—The MIT Microengine Project," AIAA Paper No. 97-1773.
[2] Isomura, K., Kawakubo, T., and Murayama, M., 2001, "Feasibility Study of a Gas Turbine at Micro Scale," ASME Paper No. 2001-GT-0101.
[3] Peirs, J., Reynaerts, D., and Verplaetsen, F., 2003, "Development of an Axial Microturbine for a Portable Gas Turbine Generator," J. Micromech. Microeng., **13**(4), pp. S190–S195.
[4] Piekos, E. S., 2000, "Numerical Simulation of Gas-Lubricated Journal Bearings for Microfabricated Machines," Ph.D. dissertation, Massachusetts Institute of Technology, Cambridge, MA.
[5] Lee, Y. B., Kwak, H. D., Kim, C. H., and Lee, N. S., 2005, "Numerical Prediction of Slip Flow Effect on Gas-Lubricated Journal Bearings for MEMS/MST-Based Micro-Rotating Machinery," Tribol. Int., **38**(1), pp. 89–96.
[6] Zhang, H. J., Zhu, C. S., and Tang, M., 2010, "Effects of Rarefaction on the Characteristics of Micro Gas Journal Bearings," J. Zhejiang Univ. Sci. A, **11**(1), pp. 43–49.
[7] Zhang, W. M., Zhou, J. B., and Meng, G., 2011, "Performance and Stability Analysis of Gas-Lubricated Journal Bearings in MEMS," Tribol. Int., **44**(7–8), pp. 887–897.
[8] Zhang, X. Q., Wang, X. L., Liu, R., and Wang, B., 2013, "Influence of Temperature on Nonlinear Dynamic Characteristics of Spiral Grooved Gas-Lubricated Thrust Bearing-Rotor Systems for Microengine," Tribol. Int., **61**, pp. 138–143.
[9] Sears, F. W., 1956, *An Introduction to Thermodynamics, the Kinetic Theory of Gases, and Statistical Mechanics*, Addison-Wesley Publishing Co., Boston, MA.
[10] Vergaftik, N. B., 1975, *Tables on the Thermophysical Properties of Liquids and Gases*, Wiley, New York.
[11] Lawrence, N. C., 1967, *Thermodynamic Properties and Reduced Correlations for Gases*, Gulf Publishing Co., Houston, TX.
[12] Din, F., 1956, *Thermodynamic Functions of Gases*, Butterworths Scientific Publications, London.
[13] Kennard, E. D., 1938, *Kinetic Theory of Gases*, McGraw-Hill, New York.
[14] Lee, D., and Kim, D., 2010, "Thermohydrodynamic Analyses of Bump Air Foil Bearings With Detailed Thermal Model of Foil Structures and Rotor," ASME J. Tribol., **132**(2), p. 021704.
[15] Zhang, H. J., Zhu, C. S., and Yang, Q., 2009, "Steady Characteristics of Micro Gas Journal Bearings Based on Rarefaction Effect," Chin. J. Theor. Appl. Mech., **41**(6), pp. 941–946.